Conference Paper

# Mathematical Modeling of Plankton Biomass Dynamics During the Spring Thermal Bar in Kamloops Lake

B O Tsydenov

Computational Geophysics Laboratory, Tomsk State University, 36 Lenin Ave., Tomsk 634050, Russian Federation

## Abstract

The mathematical model developed for simulating hydrobiological processes in a lake takes into account the diurnal variability of the heat fluxes and wind stress on the water surface. Study of the interaction of the biological components is accomplished by using the nutrient–phytoplankton–zooplankton–detritus model of Parker. The results of numerical modeling of plankton biomass dynamics during the development of the spring riverine thermal bar in Kamloops Lake, British Columbia, Canada, are presented. The data obtained have shown that the variable heat flux has a great influence on phytoplankton concentrations in the upper layers of the lake. At the presence of wind stress, zooplankton populations increase by transport from the river mouth, but concentrations of phytoplankton reduce due to the supply of colder waters from the open lake.

Corresponding Author:
B O Tsydenov
tsydenov@math.tsu.ru

Received: 10 February 2018
Accepted: 14 April 2018
Published: 7 May 2018

Publishing services provided by Knowledge E



Selection and Peer-review under the responsibility of the RFYS Conference Committee.



## 1. Introduction

A thermal bar exists in temperate lakes in spring and autumn. This phenomenon represents a narrow area where maximum density waters sink from the surface to the bottom. The thermal bar has a drastic effect on the lake's ecosystem, as it divides the body of water into zones with different temperature and hydrobiological conditions and provides a barrier to horizontal water exchange. Also it is known that the local maximum of plankton biomass is concentrated in the region of the thermal bar [1, 2].

Modeling dynamics of plankton ecology during the thermal bar events setting the constant heat flux on the water surface was implemented for Lake Baikal [3] and Lake Kamloops [4]. However, numerical study of the changes of plankton populations in the vicinity of the thermal bar is seriously limited by a lack of spatially and temporally high-resolution field observations [5]. Information obtained by simulations is of substantive importance for the purpose of determining the factors influencing the plankton growth, since plankton are an indicator of water quality and source of food to many fish species.

Currents in lakes are produced by water and atmosphere interactions. Heat transfer between the lake and the atmosphere arises through the radiative (short- and longwave radiation) and turbulent (latent and sensible heat) fluxes [6]. Shortwave radiation comes from the sun (wavelength 0.1–4 $\mu$m), and longwave radiation is emitted by the atmosphere and water surface (wavelength 4–120 $\mu$m). The latent heat flux is associated with evaporation or condensation of moisture; the sensible heat flux is generated by the temperature differences between water and near-surface air. Heat fluxes play an important role in the formation of the thermal bar in the spring-summer period because they contribute to the warming of lake surface layers up to the temperature of maximum density, close to 4 °C. Usually, for thermal bar simulating a constant heat flux is set on the lake free surface corresponding to the monthly mean value of the solar radiation [4, 7].

This study aims to simulate of hydrobiological processes based on the nutrient–phytoplankton–zooplankton–detritus model of Parker [8] during the spring riverine thermal bar in Kamloops Lake, using the non-hydrostatic model that considers daily variation of the atmospheric factors, including the wind effects, and real morphometric and hydrochemical conditions.

## 2. Mathematical model and numerical method

The non-hydrostatic mathematical model consists of the thermohydrodynamic (subsection 2.1) and hydrobiological (subsection 2.2) submodels with initial and boundary conditions (subsections 2.3 and 2.4). The equations of the model are solved numerically (subsection 2.5).

### 2.1. Equations of the thermohydrodynamic submodel

The thermohydrodynamic submodel includes momentum, continuity, and energy equations and an equation of salinity balance in the lake [9]:

$$\frac{\partial u}{\partial t}+\frac{\partial u^2}{\partial x}+\frac{\partial uw}{\partial z}=-\frac{1}{\rho_0}\frac{\partial p}{\partial x}+\frac{\partial}{\partial x}\left(K_x\frac{\partial u}{\partial x}\right)+\frac{\partial}{\partial z}\left(K_z\frac{\partial u}{\partial z}\right)+2\Omega_z v-2\Omega_y w; \quad (1)$$

$$\frac{\partial v}{\partial t}+\frac{\partial uv}{\partial x}+\frac{\partial wv}{\partial z}=\frac{\partial}{\partial x}\left(K_x\frac{\partial v}{\partial x}\right)+\frac{\partial}{\partial z}\left(K_z\frac{\partial v}{\partial z}\right)+2\Omega_x w-2\Omega_z u; \quad (2)$$

$$\frac{\partial w}{\partial t}+\frac{\partial uw}{\partial x}+\frac{\partial w^2}{\partial z}=-\frac{1}{\rho_0}\frac{\partial p}{\partial z}+\frac{\partial}{\partial x}\left(K_x\frac{\partial w}{\partial x}\right)+\frac{\partial}{\partial z}\left(K_z\frac{\partial w}{\partial z}\right)-\frac{g\rho}{\rho_0}+2\Omega_y u-2\Omega_x v; \quad (3)$$

$$\frac{\partial u}{\partial x}+\frac{\partial w}{\partial z}=0; \quad (4)$$

$$\frac{\partial T}{\partial t}+\frac{\partial uT}{\partial x}+\frac{\partial wT}{\partial z}=\frac{\partial}{\partial x}\left(D_x\frac{\partial T}{\partial x}\right)+\frac{\partial}{\partial z}\left(D_z\frac{\partial T}{\partial z}\right)+\frac{1}{\rho_0 c_p}\frac{\partial H_{sol}}{\partial z}; \quad (5)$$

$$\frac{\partial S}{\partial t}+\frac{\partial uS}{\partial x}+\frac{\partial wS}{\partial z}=\frac{\partial}{\partial x}\left(D_x\frac{\partial S}{\partial x}\right)+\frac{\partial}{\partial z}\left(D_z\frac{\partial S}{\partial z}\right), \quad (6)$$

where $u$, $v$ are the horizontal velocity components; $w$ is the vertical velocity component; $\Omega_x$, $\Omega_y$and $\Omega_z$ are the vector components of the angular velocity of Earth's rotation; $K_x$($D_x$)and $K_z$ ($D_z$) are the eddy viscosity (diffusivity) coefficients in the horizontal and vertical directions, respectively; $g$ is the acceleration of gravity; $c_p$ is the specific heat capacity; $T$ is the temperature; $S$ is the salinity; $p$ is the pressure; and $\rho_0$ is the water density at standard atmospheric pressure, temperature $T_L$ and salinity $S_L$ ($T_L$ and $S_L$ are a reference temperature and salinity of the lake, respectively). Wilcox's two-parameter k–ω turbulence model [10] consisting of equations for kinetic energy and turbulent fluctuation frequency and algebraic relations to find eddy diffusivity [11] are used to close the set of equations (1)–(6). The Chen–Millero equation [12] connecting water density with temperature, salinity, and pressure and valid within the range of 0 ≤ $T$≤ 30°C, 0 ≤ $S$≤ 0.6 g kg$^{-1}$, 0 ≤ $p$≤ 180 bar was taken as the state equation.

## 2.2. Equations of the hydrobiological submodel

The transport of plankton components is described by the convection–diffusion equations

$$\frac{\partial \Psi}{\partial t}+\frac{\partial u\Psi}{\partial x}+\frac{\partial w\Psi}{\partial z}=\frac{\partial}{\partial x}\left(D_x\frac{\partial \Psi}{\partial x}\right)+\frac{\partial}{\partial z}\left(D_z\frac{\partial \Psi}{\partial z}\right)+S_\Psi, \quad (7)$$

where Ψ is the concentration of the biological component (nutrient, phytoplankton, zooplankton, and detritus) and $S_\Psi$is its source term representing the result of interaction with other components. Numerical modeling of hydro-biological processes is carried out by the nutrient ($N$)–phytoplankton ($P$)–zooplankton ($Z$)–detritus ($D$) model of Parker [8]. The computation formulas defining the value of each source term are presented in table 1.

G represents the phytoplankton primary production rate and is calculated as:

$G = V_m\,[(L_d/s_c)\,\exp\{1-(L_d/s_c)\},N/(N+k_s)]$.

The light at depths of $L_d$ is determined by the exponential dependence taking into account self-shading by plankton and detritus in the water column between the surface ($z$=$L_z$) and the depth ($z$=$d$):

$$L_d = L_s \exp\left\{-\eta d - S_s\int_d^{L_z}(P+Z+D)\,dz\right\}.$$

Table 1: Interactions between the nutrient, phytoplankton, zooplankton, and detritus.

| Source term | Computation formula |
|---|---|
| $S_P$ | $P(G - m_P - IZ)q$ |
| $S_Z$ | $Z[(1 - \gamma_N - \gamma_D)IP - m_Z]q$ |
| $S_N$ | $(-GP + \gamma_N IPZ + C_0 D)q$ |
| $S_D$ | $(m_P P + \gamma_D IPZ - C_0 D + m_Z Z)q$ |

According to Sverdrup [13], the photosynthetically active radiation is 20% of the total solar energy (see subsection 2.4). On that basis, the daily insolation on the lake surface is defined.

The phytoplankton death rate and the thermal limitation factor are calculated

$m_P = M\ exp\{-(n_1 N)^2\};$

$q = 2.5^{(T-15)/10},$

respectively.

Parameters occurring in the plankton model are listed in table 2 [4].

Table 2: Parameter values for nutrient–phytoplankton–zooplankton–detritus model.

| Parameter | Description | Value |
|---|---|---|
| $V_m$ | Maximum phytoplankton growth rate | 2.8 $day^{-1}$ |
| η | Light extinction coefficient | 0.15 $m^{-1}$ |
| $k_s$ | Nutrient uptake half-saturation constant | 0.6 mmol N $m^{-3}$ |
| $m_Z$ | Zooplankton death rate | 0.1 $day^{-1}$ |
| $I$ | Ingestion rate of zooplankton | 0.2 $day^{-1}$ |
| $M$ | Maximum phytoplankton death rate | 0.5 $day^{-1}$ |
| $n_1$ | Phytoplankton death rate coefficient | 1 (mmol N $m^{-3}$)$^{-1}$ |
| $\gamma_N$ | Unassimilated zooplankton grazing to nutrients | 0.4 |
| $\gamma_D$ | Unassimilated zooplankton grazing to detritus | 0.3 |
| $C_0$ | Detritus to nutrient conversion rate | 0.02 $day^{-1}$ |
| $S_s$ | Self-shading coefficient | 0.02 (mmol N $m^{-3}$)$^{-1}m^{-1}$ |
| $s_c$ | Light saturation coefficient | 60 Einstein $m^2 day^{-1}$ |

## 2.3. Initial and boundary conditions

Initial conditions for equations (1)–(6) are set as:

$u = 0;\ \ v = 0;\ \ w = 0;\ \ T = T_L;\ \ S = S_L;\ \ \Psi = \Psi_L$ at $t$= 0,

where $T_L$, $S_L$,$\Psi_L$ are the temperature, salinity, and concentration of the biological component in the lake, respectively; $t$ is the time. The initial pressure field is found through the state and hydrostatic equations with the boundary condition $p$=$p_a$ on the surface by a fourth-order Runge–Kutta method.

Boundary conditions for equations (1)–(6) are as follows:

- at the free surface

$$\frac{\partial u}{\partial z} = 0;\ \frac{\partial v}{\partial z} = 0;\ w = 0;\ D_z\frac{\partial T}{\partial z} = \frac{H_{net}}{\rho_0 \cdot c_p};\ \frac{\partial S}{\partial z} = 0;\ \frac{\partial \Psi}{\partial z} = 0,$$

where heat flux $H_{net}$ is composed of the longwave radiation and latent and sensible heat (see subsection 2.4);

- at the solid boundaries

$$u = 0;\ v = 0;\ w = 0;\ \frac{\partial T}{\partial n} = 0;\ \frac{\partial S}{\partial n} = 0;\ \frac{\partial \Psi}{\partial n} = 0,$$

where $n$is the direction of the outward normal to the domain;

- at the river inflow boundary

$$u = u_R;\ v = 0;\ w = 0;\ T = T_R;\ S = S_R;\ \Psi = \Psi_R,$$

where $u_R$ is the river inflow velocity; $T_R$, $S_R$,$\Psi_R$ are the temperature, salinity, and concentration of the biological component in the river, respectively; and

- at the open boundaryradiation type conditions are set [14]

$$\frac{\partial \varphi}{\partial t} + c_\varphi\frac{\partial \varphi}{\partial x} = 0 \quad (\varphi = u, v, T, S, \Psi)$$

and simple gradient conditions are

$$\frac{\partial w}{\partial x} = 0.$$

## 2.4. Heat fluxes on the surface of the lake

Parameterization of the longwave radiation ($H_{lw}$) and fluxes of latent ($H_L$) and sensible ($H_S$) heat is carried out by the model number 3 from [15]:

- $H_{lw} = \epsilon_w\epsilon_a\sigma\left(1 + 0.17C^2\right)T_A^4 - \epsilon_w\sigma T^4$,

where $T_A$ is the air temperature, K; $T$ is the water temperature, K; $C$ is the cloud amount as a fraction; σ = 5.669×10$^{-8}$ W/m$^2$/K$^4$ is the Stefan-Boltzmann constant; and $\varepsilon_w \approx$ 0.97is the water emissivity. The atmospheric emissivity is calculated by the formula

$$\epsilon_a = C_\epsilon T_A^2,$$

here $C_\varepsilon$=9.37×10$^{-6}$°C$^{-2}$ is the emissive power of air;

- $H_L = f_u\left(e_A - e_w\right)$;

$$f_u = 6.9 + 0.345 \cdot U_{10}^2;$$

$$e_w = 6.112 \exp\left(\frac{17.67 \cdot T_A^C}{T_A^C + 243.5}\right),$$

where $e_w$ is the pressure of saturated water vapor, hPa; $e_A$=0.01·$RH$·$e_w$ is the pressure of water vapor in the atmosphere, hPa; $RH$ is the relative humidity, %; $f_u$ is the heat-transfer coefficient, W m$^{-2}$ hPa$^{-1}$; $U_{10} = \sqrt{u_{10}^2 + v_{10}^2}$ is the wind speed, m s$^{-1}$; and $T^C$ is the air temperature, °C; and

- $H_S = \beta \cdot f_u\left(T_A - T\right)$,

where $H_{lw}$ is the longwave radiation; and $H_L$, $H_S$ are the fluxes of latent and sensible heat, respectively.

Shortwave radiation absorption $H_{sol}$ is calculated according to the Beer–Lambert–Bouguer law:

$$H_{sol} = H_{Ssol,0}\left(1 - r_s\right)\exp\left(-\epsilon_{abs} \cdot d\right),$$

where $d = |L_z - z|$is the depth, $r_s \approx$0.2is the water reflectivity coefficient, and $\varepsilon_{abs} \approx$0.3 m$^{-1}$is the solar radiation absorption coefficient in water. Solar radiation influx at the lake surface $H_{Ssol,0}$ is calculated from the following equation:

$$H_{Ssol,0} = \begin{cases} S_0 \cdot \left(a_g - a_w\right) \cdot \cos\zeta \left[a(C) + b(C)\ln(\cos\zeta)\right], & \text{if } \cos\zeta > 0; \\ 0, & \text{if } \cos\zeta \le 0, \end{cases}$$

where $S_0 \approx$1367W m$^{-2}$ is the solar constant, $a(C)$ and $b(c)$ are the empirical coefficients [16], $\zeta$is the solar zenith angle, and the empirical functions

$a_g = 0.485 + 0.515 \cdot \left(1.014 - 0.16/\sqrt{\cos\zeta}\right)$ and

$$a_w = 0.039 \cdot \left(r_w/\cos\zeta\right)^{0.3}$$

represent respectively molecular scattering and absorption by permanent gases; and $r_w$ is the water vapor content in the atmosphere, kg m$^{-2}$.

### 2.5. Numerical method

The numerical solution of the problem is based on the finite volume method according to which scalar values (concentrations of the nutrient, phytoplankton, zooplankton, and detritus; water temperature, salinity, and pressure; and turbulent diffusion coefficients) are determined in the center of the grid cell while wind velocity components are in the middle points at the cell boundaries. In order to approximate the computational domain to the lake's actual topography, the fictitious domain method is used: the velocity components in a dead zone are set to zero by using large values of the viscosity coefficients in this zone [17].

The numerical algorithm for finding the flow and temperature fields is based on a Crank–Nicolson difference scheme. The convective terms in the equations are approximated with a second-order upstream scheme, QUICK [18]. To correlate the calculated velocity and pressure fields, a procedure for buoyant flows, SIMPLED (Semi-Implicit Method for Pressure Linked Equations with Density correction) [9], which is a modification of Patankar's method SIMPLE [17], has been developed. SIMPLED corrects velocity and pressure fields by accounting for the variation in density in the gravitational term in equation (3). The systems of grid equations at each time step are solved by the under-relaxation method.

## 3. Research area and computation conditions

The study area is Kamloops Lake, located in Southwestern Canada, British Columbia, 340 km northeast of Vancouver, between 50°26′ – 50°45′ N and 120°03′ – 120°32′ W, on the Thompson River.

A vertical cross-section of Kamloops Lake along the Thompson River inflow is taken for this numerical experiment. The origin of the system of coordinates coincides with the river mouth (Figure 1a). The calculation domain is 10 km long and 138 mdeep (Figure 1b). The depth of the river inflow is 15 m. The calculation domain (Figure 1b) is covered by a uniform orthogonal grid with dimensions $h_x$=25 m and $h_z$=3 m. The time step Δt=60 s.

Initial temperature distribution in Kamloops Lake has a constant value equal to 2.4°C while water temperature in the river corresponds to 3.6°C and increases by 0.2°C per day. The Thompson River falls into the lake with a velocity of 0.01 m $s^{-1}$, and water mineralization in the lake and river is 0.1 g $kg^{-1}$. Initial concentration of the nutrient,

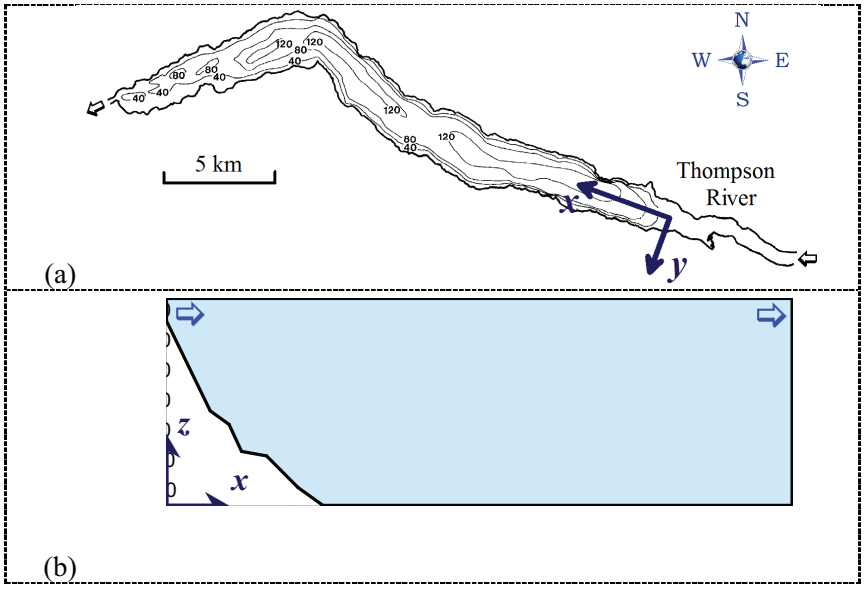


**Figure** 1: Kamloops Lake morphometry: (a) bathymetry, (b) calculation domain (longitudinal section).

phytoplankton, zooplankton, and detritus is 4.0, 1.0, 1.0, and 1.0 mmol N $m^{-3}$, respectively [4].

## 4. Results and discussion

The data on the air temperature, relative humidity, atmospheric pressure, cloudiness [19], wind speed and wind direction (Figure 2; the meteorological measurements are indicated by symbols) from the meteorological conditions archive of the station of City of Kamloops (50°41′ N, 120°20′ W) for the period 01.04.2015–30.04.2015 (http://climate.weather.gc.ca) are used in the calculation of longwave radiation and latent and sensible heat fluxes.

The analysis of wind data (Figure 2) indicates that the gusts of wind achieve 10–12 m $s^{-1}$ in April 2015. Strong wind load on the surface of Kamloops Lake is for the days 10–14 of the month. Therewith, at this time interval the westerly winds prevail.

During April 2015 the longwave radiation was predominantly negative and oriented to cooling of lake surface (Figure 3). The values of the latent heat flux fluctuated between –206 and –5 W $m^{-2}$, and the minimum was observed on the $21^{st}$ day of the month (Figure 3). The sensible heat flux varies from –17 to 116 W $m^{-2}$(Figure 3). The shortwave (solar) radiation is the most important component, providing the major contribution to the heat exchange and increasing during the daytime to the maximum value of 673 W $m^{-2}$. The total heat influence on the lake water is composed of all four

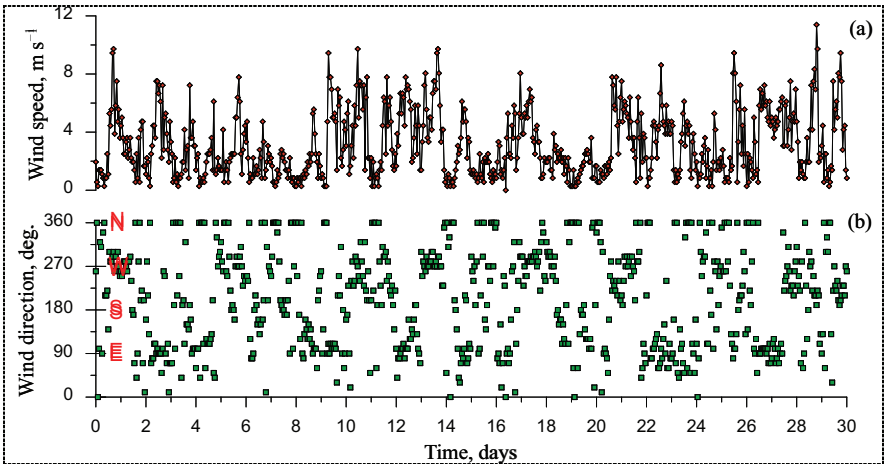


**Figure** 2: Wind speed (a) and wind direction (b) of wind from 1 to 30 April 2015 (local standard time).

components of the heat fluxes. Average value of the total flux in April 2015 was 114 W m$^{-2}$.

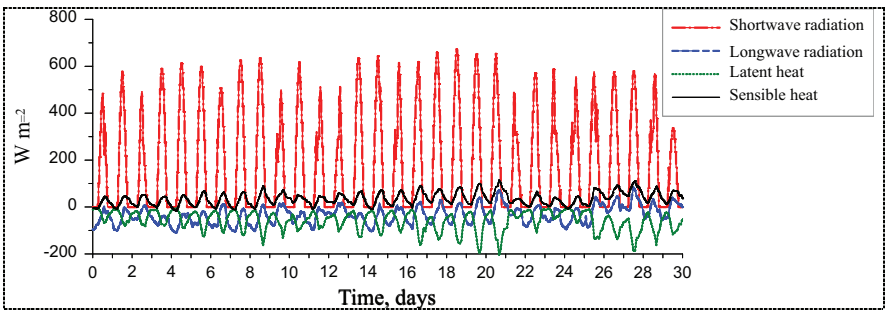


**Figure** 3: Heat flux components calculated from 1 to 30 April 2015 (local standard time).

The maximum density temperature contour demonstrates the velocity of the thermal bar propagation at the lake surface. Figure 4 illustrates the dynamics of thermal bar development based on the position of the temperature of maximum density (TMD) provided a constant monthly average value of the total heat flux equal to 117 W m$^{-2}$ and the variable heat flux with wind and without wind. The location of the maximum density temperature (Figure 4) shows that the thermal bar is formed on the fourth day of simulation. By comparing the diagrams in Figure 4, we can conclude that the boundary condition with the variable heat flux on the free surface (without wind) affects the process of thermal bar evolution, especially during the night cooling, which reduces the velocity of the thermal bar movement. However, the wind has the most impact on the thermal bar development. The strong prolonged westerly winds blowing opposite to the direction of the thermal bar propagation can produce reverse movement of the thermobaric front (Figure 4, see days 10, 13, 15, etc.).

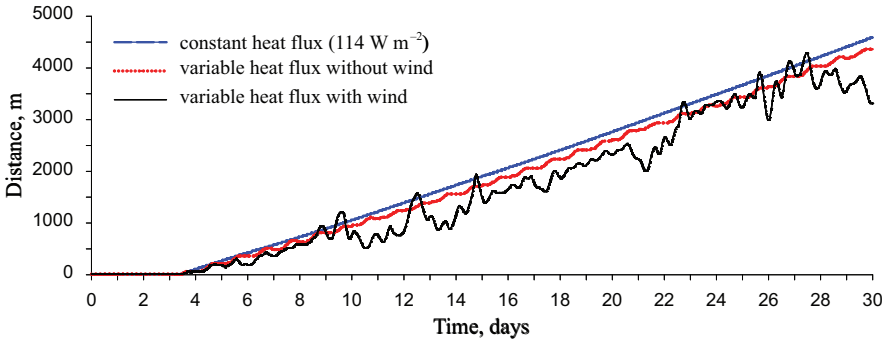


**Figure** 4: Dynamics of horizontal displacement of maximum density temperature at the lake surface.

The location of 4 °C isotherm (the temperature of maximum density) indicates that the thermal bar front is approximately 600 m from the Thompson River mouth on the 8th day of the model run (Figure 5a1) and shifts to 1 900 m on the 16th day (Figure 5a2). It is obvious that on day 8 phytoplankton populations begin to grow in the area of the river mouth (Figure 5c1). Further ingress of warmer riverine waters into the lake leads to a rapid rise in the phytoplankton biomass (Figure 5c2), which results in the degradation of the nutrient in corresponding zone (Figure 5b). It is important to note that the maximum growth of the phytoplankton is in the near-surface layers of thermoactive region (i.e. the inshore side of the thermal bar). The downwelling plume arising inside of the thermal bar front carries off the zooplankton (Figure 5d) and detritus (Figure 5e) in the deeper part of the lake.

The time-spatial distribution of the biological components within the front of the thermal bar shows that the phytoplankton biomass actively grows in the lake's upper layers (Figure 6a). Zooplankton populations tend to decrease during the evolution of the thermal bar (Figure 6b). Variable heat flux strongly influences the intraday changes of phytoplankton concentrations near the lake surface (Figure 6a2). But, according to Parker's model no major differences in concentrations of zooplankton were observed (compare Figure 6b1 and Figure 6b2), as in the case of using the model of Franks et al. (Figure 6b in [19]).

Numerical modeling has discovered that wind has a significant effect on the distribution of phytoplankton and zooplankton biomasses (Figure 7). At the presence of wind stress on the water surface, the gradients of plankton concentrations are weak (Figure 7a1, Figure 7b1). The reason – mixing of waters due to horizontal near-surface flows induced by wind friction. Under this condition, concentrations of zooplankton in the lake increase by transport from the river mouth (Figure 7b1), but concentrations of phytoplankton reduce due to water temperature decrease in the near-shore area, owing to the supply of colder waters from the open lake (Figure 7a1). Windless state

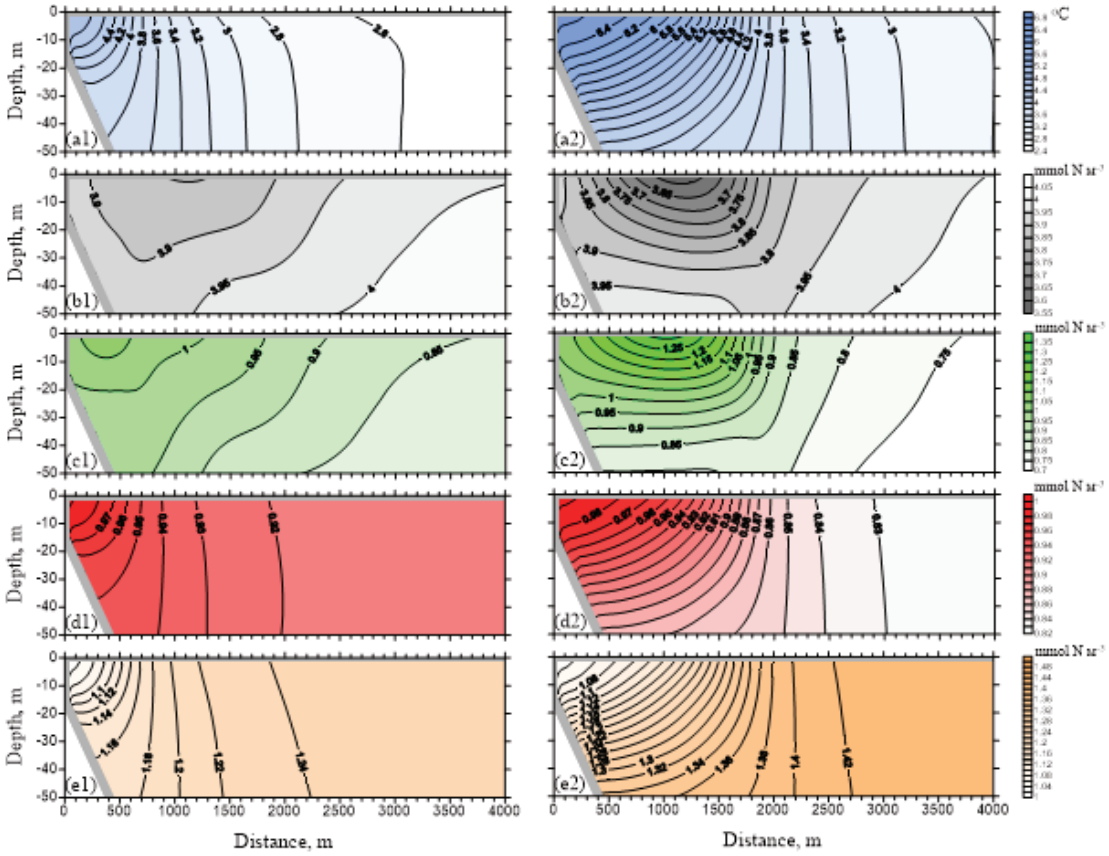


**Figure** 5: Isotherms (a); concentrations of nutrient (b), phytoplankton (c), zooplankton (d), and detritus (e) on day 8 (1) and day 16 (2).

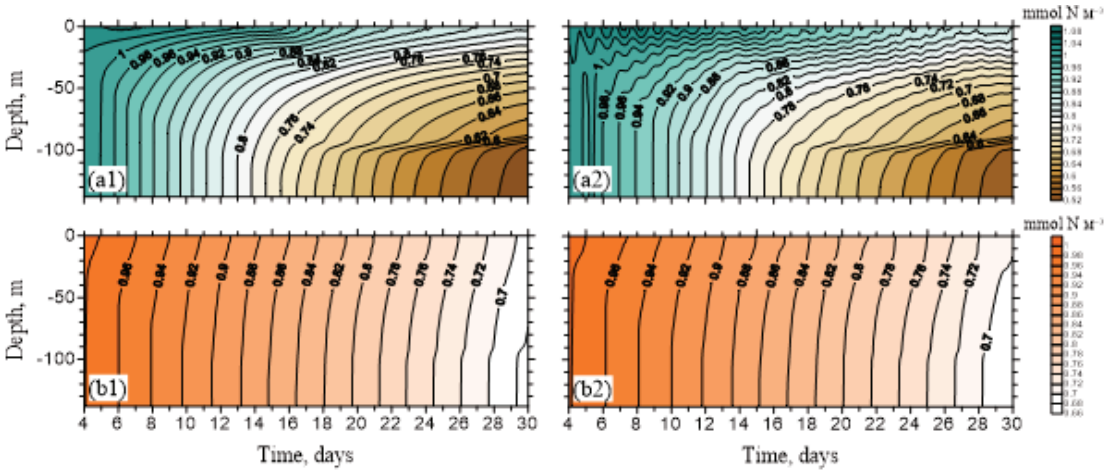


**Figure** 6: Isopleths of phytoplankton (a) and zooplankton (b) concentration as a function of time and depth at $x=x_{TMD}$ with constant (1) [114 W m$^{-2}$] and variable (2) heat fluxes.

of the atmosphere has a positive effect on growth of phytoplankton population and on day 12 of simulation the maximum value of phytoplankton concentrations is at a distance of 700 m from the mouth of the Thompson River (Figure 7a2).

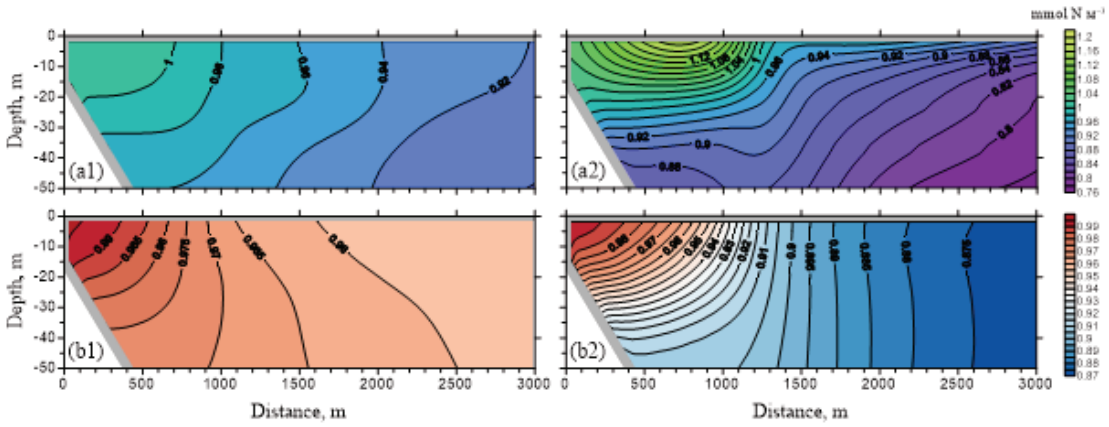


**Figure** 7: Concentrations of phytoplankton (a) and zooplankton (b) on day 12 with wind (1) and without wind (2).

## 5. Conclusions

Mathematical modeling of plankton dynamics during the thermal bar events based on the model of Parker considering the self-shading and temperature dependence factors has demonstrated that the diurnal variability of the meteorological parameters has a significant impact on plankton populations. It has been numerically established that the variable heat flux gives higher values for concentrations of phytoplankton during daylight hours. In addition, wind initiates mixing of near-surface waters, which has a negative effect on the growth of phytoplankton and assists in transport of zooplankton from the river mouth.

## Acknowledgments

The reported study was funded by RFBR, according to the research project No. 16-31-60041 mol_a_dk. The author is very grateful to Jean Kollantai, Senior Lecturer at Tomsk State University, for style review.

## References

[1] Parfenova V V, Shimaraev M N, Kostornova T Ya, Domysheva V M, Levin L A, Dryukker V V, Zhdanov A A, Gnatovskii R Yu, Tsekhanovskii V V and Logacheva N F 2000 *Microbiology* **69** 357–63.

[2] Mortimer C H 1974 *Mitt. Int. Ver. Limnol.* **20** 124–97.

[3] Botte V and Kay A 2000 *J. Mar. Sys.* **26** 367–86.

[4] Holland P R, Kay A and Botte V 2003 *J. Mar. Syst.* **43** 61–81.

[5] Holland P R and Kay A 2003 *Limnologica* **33** 153–62.
[6] Ji Zh G 2007 *Hydrodynamics and Water Quality: Modeling Rivers, Lakes, and Estuaries* (New York: John Wiley & Sons).
[7] Vasiliev O F, Bocharov O B, Kvon V I, Ovchinnikova T E and Kvon D V 1998 *Proc. 3 Int. Conf. on Hydro-Science and Engineering (Electronic Materials)* (Cottbus/Berlin) p 20.
[8] Parker R A 1991 *J. Plankton Res.* 1991 **13** 815–30.
[9] Tsydenov B O, Kay A and Starchenko A V 2016 *Ocean Modelling* **104** 73–83.
[10] Wilcox D 1988 *AIAA J.* **26** 1299–310.
[11] Tsydenov B O and Starchenko A V 2014 *Vestn. Tomsk. Gos. Univ. Mat. Mekh.* **5** 104–13.
[12] Chen C and Millero F 1986 *Limnol. Oceanogr.* **31** 657–62.
[13] Sverdrup H 1953 *J. du Conseil Int. pour l'Exploration de la Mer.* **18** 287–95.
[14] Orlanski I 1976 *J. Comput. Phys.* **21** 251–69.
[15] Tsydenov B O and Starchenko A V 2015 *Proc. SPIE* **9680** 96800H.
[16] Aleksandrova M P, Gulev S K and Sinitsyn A V 2007 *Russian Meteorology and Hydrology* **32** 245–51.
[17] Patankar S 1980 *Numerical heat transfer and fluid flow* (Washington DC: Hemisphere Publishing Corp.) p 210.
[18] Leonard B 1979 *Computer Methods in Applied Mechanics and Engineering* **19** 59–98.
[19] Tsydenov B 2016 *Proc. SPIE* **10035** 1003503.